



**HAL**  
open science

# Near-Infrared Lanthanide-Based Emission from Fused Bis[Ln(III)/Zn(II) 14-metallacrown-5] Coordination Compounds

John Karns, Svetlana Eliseeva, Cassandra Ward, Matthew Allen, Stephane Petoud, Jacob Lutter

► **To cite this version:**

John Karns, Svetlana Eliseeva, Cassandra Ward, Matthew Allen, Stephane Petoud, et al.. Near-Infrared Lanthanide-Based Emission from Fused Bis[Ln(III)/Zn(II) 14-metallacrown-5] Coordination Compounds. *Inorganic Chemistry*, 2022, 61 (15), pp.5691-5695. 10.1021/acs.inorgchem.2c00084 . hal-03652821

**HAL Id: hal-03652821**

**<https://hal.science/hal-03652821>**

Submitted on 27 Apr 2022

**HAL** is a multi-disciplinary open access archive for the deposit and dissemination of scientific research documents, whether they are published or not. The documents may come from teaching and research institutions in France or abroad, or from public or private research centers.

L'archive ouverte pluridisciplinaire **HAL**, est destinée au dépôt et à la diffusion de documents scientifiques de niveau recherche, publiés ou non, émanant des établissements d'enseignement et de recherche français ou étrangers, des laboratoires publics ou privés.

# Near-infrared lanthanide-based emission from fused bis[Ln(III)/Zn(II) 14-metallacrown-5] coordination compounds.

*John P. Karns,<sup>a</sup> Svetlana V. Eliseeva,<sup>b,\*</sup> Cassandra L. Ward,<sup>c</sup> Matthew J. Allen,<sup>a</sup> Stéphane*

*Petoud<sup>b,\*</sup> and Jacob C. Lutter<sup>a,\*</sup>*

<sup>a</sup> Department of Chemistry, Wayne State University, Detroit, MI, 48202, USA.

<sup>b</sup> Centre de Biophysique Moléculaire, CNRS UPR 4301, 45071 Orléans Cedex 2, France.

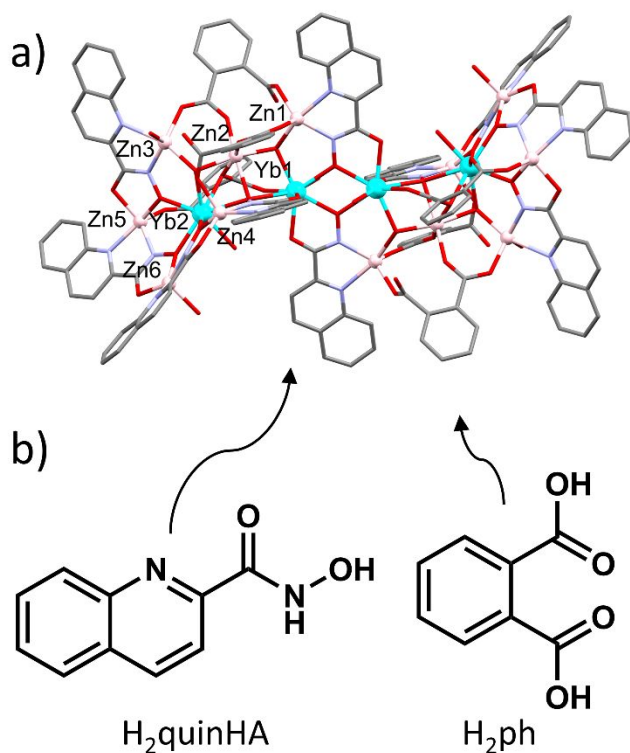
<sup>c</sup> Lumingen Instrument Center, Wayne State University, Detroit, MI, 48202, USA.

Lanthanides, Near-infrared, Luminescence, Metallacrowns, Heterobimetallic Complexes, Single-crystal X-ray Diffraction

A set of  $(\text{Ln}[14\text{-MC}_{\text{Zn}}^{(\text{II})}_{\text{N}(\text{quinHA})\text{-5}}])_2\text{Ln}_2\text{Zn}_2(\text{quinHA})_2(\text{ph})_2(\text{Hph})_4(\text{OH})_8(\text{H}_2\text{O})_4$  metallacrowns (**Ln-1**, Ln = Tb, Gd, or Yb; H<sub>2</sub>quinHA = quinaldic hydroxamic acid, H<sub>2</sub>ph = phthalic acid) have been synthesized via solution-state self-assembly. The MCs possess an uncommon topology within the metallacrown family where two rarely seen 14-metallacrown-5 moieties are fused by a Yb<sub>2</sub>Zn<sub>2</sub>(quinHA)<sub>2</sub> bridge. Moreover, **Yb-1** analyzed in the solid state exhibits a characteristic near-IR luminescence signal arising from Yb<sup>3+</sup> <sup>2</sup>F<sub>5/2</sub>→<sup>2</sup>F<sub>7/2</sub> transition despite the proximity of high energy O–H oscillators.

Compounds formed with trivalent lanthanide cations (Ln<sup>3+</sup>) possess unique magnetic and luminescence properties that are examined across a variety of fields.<sup>1,2</sup> These properties result from 4f valence electrons that are shielded from their environment by filled 5s and 5p orbitals.<sup>3</sup> From a magnetic perspective, Ln<sup>3+</sup> have been studied as single-molecule magnets, thanks to unquenched spin-orbit coupling that enhances anisotropy, and as contrast agents for magnetic resonance imaging.<sup>4-9</sup> From a luminescence point of view, Ln<sup>3+</sup> are attractive because of their characteristic and narrow emission bands, as well as their long luminescence lifetimes.<sup>3,10-15</sup> In addition, several Ln<sup>3+</sup> ions emit photons in the near-IR spectroscopic range that are of special interest for deep tissue imaging and telecommunications.<sup>10</sup> However, Ln<sup>3+</sup> have low absorbance because most f–f

transitions are parity forbidden. To counteract this limitation organic chromophoric ligands with large molar absorption coefficients can be used to sensitize  $\text{Ln}^{3+}$  via energy transfer, leading to enhanced emission (antenna effect).<sup>16,17</sup>



**Figure 1.** Representation of the molecular structure of **Yb-1** from single crystal diffraction data (a), and schematic representation of the two parent ligands: quinaldic hydroxamic acid (H<sub>2</sub>quinHA) and phthalic acid (H<sub>2</sub>ph) (b). Aqua = Yb, pink = Zn, light blue = N, red = O, grey = C. Solvent molecules and hydrogen atoms are omitted for clarity.

Metallacrowns (MCs) were first introduced by Pecoraro and Lah in 1989 as inorganic analogues to crown ethers, where the  $[-C-C-O-]_n$  repeating unit is replaced by a  $[-M-N-O-]_n$  unit to form a rigid macrocycle.<sup>18,19</sup> M is typically a third-row metal ion, and the N–O binding unit is usually provided by hydroximates.<sup>20–22</sup> Since 2011, MCs have been studied as antenna for  $Ln^{3+}$ ,<sup>23</sup> typically including optically silent metals such as  $Zn^{2+}$  and  $Ga^{3+}$  to form the metallamacrocycle structure. Such  $Ln^{3+}$ -based MCs have shown promises for optical imaging, orthogonal functionalization, nanothermometry, and white-light emission.<sup>24–33</sup> Here, we present a series of  $Ln^{3+}/Zn^{2+}$  MCs ( $Ln[14-MC_{Zn}^{II}N(quinHA)-5]_2Ln_2Zn_2(quinHA)_2(ph)_2(Hph)_4(OH)_8(H_2O)_4$  (**Ln-1**, Ln = Tb, Gd, or Yb;  $H_2quinHA$  = quinaldic hydroxamic acid,  $H_2ph$  = phthalic acid, **Figure 1**) possessing a different structure that hasn't been reported so far. They contain two fused [14-MC-5] motifs and are able to sensitize  $Yb^{3+}$  luminescence in the near-IR range.


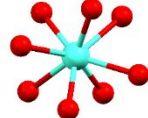


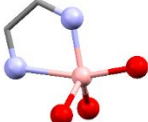
The self-assembly synthesis of **Ln-1** compounds was achieved via a stoichiometric addition of the appropriate components in *N,N*-dimethylformamide. A diffusion of water into *N,N*-dimethylformamide solutions of **Ln-1** formed single crystals. X-ray diffraction confirmed the same unit cell parameters for each of the series of **Ln-1**. Detailed analysis was performed on **Yb-1** that is comprised of four  $Yb^{3+}$ , twelve  $Zn^{2+}$ , ten  $quinHA^{2-}$ , four  $Hph^-$ , two  $ph^{2-}$ , eight  $OH^-$ , and four



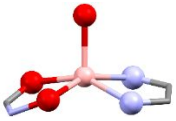
H<sub>2</sub>O. This structure contains two [14-MC-5] motifs that are spanned by a central Yb<sub>2</sub>Zn<sub>2</sub>(quinHA)<sub>2</sub> moiety (**Figures S1 and S2**, Supporting Information). The solid-state packing of **Yb-1** molecules is stabilized by through-solvent intermolecular interactions (including hydrogen bonding and van der Waals interactions) and  $\pi$ - $\pi$  stacking of adjacent quinHA<sup>2-</sup> located on neighboring molecules. Each metal ion was analyzed for its coordination geometry. In particular, coordination number (CN), shape, crystal shape measure parameter (CShM), average bond length ( $d_{av}$ ), and bond-valence sums (BVS) were determined (**Table 1**). Representations generated from the crystallographic data of each ligand field may be observed in **Table 1** and **Figure S3** (Supporting Information).

Two unique Yb<sup>3+</sup> cation sites can be distinguished, yet analysis with SHAPE v2.1 software on both Yb1 and Yb2 confirm eight-coordinate trigonal dodecahedral environments comprised of eight oxygens.<sup>34</sup> Bond-valence sums confirmed the +3 oxidation state for each of the two Yb<sup>3+</sup> cations. Yb1 is a part of the spanning moiety while Yb2 is a part of the [14-MC-5] motif. There are six Zn<sup>2+</sup> in the asymmetric unit, and all but Zn2 adopt a coordination number of five. Zn2 is in a six-coordinate octahedral coordination environment comprised of oxygen atoms. Zn1 and Zn3–Zn6 are all in five-coordinate coordination environments comprised of three oxygen and two

nitrogen donor atoms. Analysis with SHAPE v2.1 suggests that the best coordination geometry to describe Zn1 and Zn4–Zn6 is square pyramidal while Zn3 is best described as a trigonal bipyramidal geometry.<sup>34</sup> Bond-valence sums confirm the +2 oxidation state for each Zn<sup>2+</sup> cation. Zn1 is the only Zn<sup>2+</sup> cation that is a part of the spanning moiety, whereas the other five Zn<sup>2+</sup> cations are a part of the [14-MC-5] motif.

**Table 1.** Geometric information for metal cations in **Yb-1**.

| Metal | $d_{av}$ | CN  | Crystallographic Representation   | Shape                    | CShM <sup>a</sup> | BVS <sup>35,36</sup> | Addison Tau <sup>37</sup> |
|-------|----------|---|---|--------------------------|-------------------|----------------------|---------------------------|
| Yb1   | 2.321    | 8 [5 O <sub>quinHA</sub> ,<br>1 O <sub>ph</sub> , 1 O <sub>OH</sub> ,<br>1 O <sub>water</sub> ] |   | Trigonal<br>Dodecahedron | 1.01186           | 3.036                | -----                     |
| Yb2   | 2.337    | 8 [4 O <sub>quinHA</sub> ,<br>2 O <sub>ph</sub> , 1 O <sub>OH</sub> ,<br>1 O <sub>water</sub> ] |  | Trigonal<br>Dodecahedron | 0.60167           | 2.950                | -----                     |
| Zn1   | 2.066    | 5 [2 N <sub>quinHA</sub> ,<br>2 O <sub>ph</sub> , 1 O <sub>OH</sub> ]                           |  | Square<br>Pyramid        | 2.06806           | 1.988                | 0.446                     |
| Zn2   | 2.098    | 6 [1 O <sub>quinHA</sub> ,<br>3 O <sub>ph</sub> , 1 O <sub>OH</sub> ]                           |  | Octa-<br>hedron          | 1.17399           | 2.050                | -----                     |
| Zn3   | 2.074    | 5 [2 N <sub>quinHA</sub> ,<br>1 O <sub>ph</sub> , 2 O <sub>OH</sub> ]                           |  | Trigonal<br>Bipyramid    | 2.20789           | 1.995                | 0.583                     |

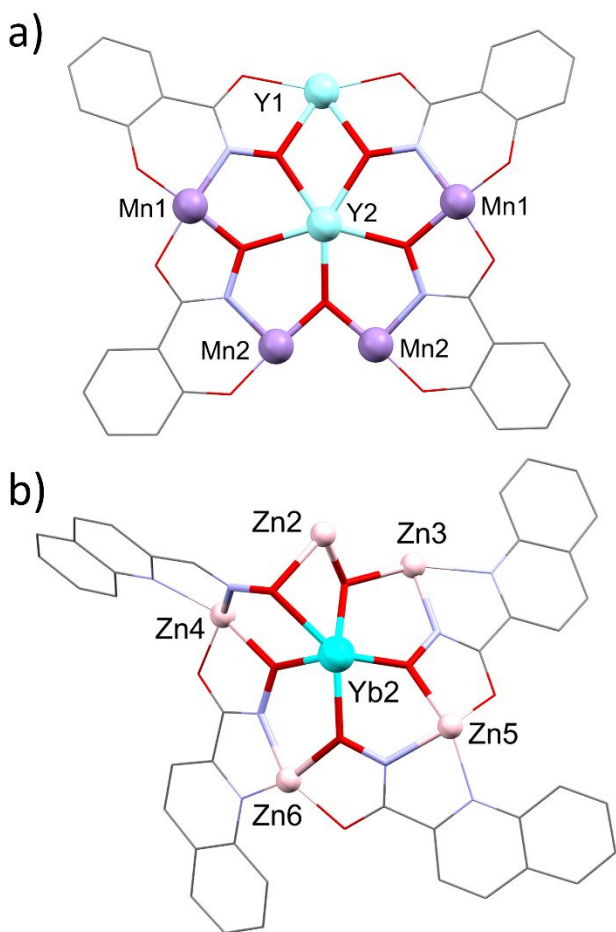
|     |       |  |   |                   |         |       |       |
|-----|-------|--|---|-------------------|---------|-------|-------|
| Zn4 | 2.052 | 5 [2 N <sub>quinHA</sub> ,<br>2 O <sub>quinHA</sub> , 1<br>O <sub>ph</sub> ]   |  | Square<br>Pyramid | 0.59023 | 2.022 | 0.110 |
| Zn5 | 2.035 | 5 [2 N <sub>quinHA</sub> ,<br>2 O <sub>quinHA</sub> , 1<br>O <sub>ph</sub> ]   |  | Square<br>Pyramid | 0.88679 | 2.113 | 0.169 |
| Zn6 | 2.048 | 5 [[2 N <sub>quinHA</sub> ,<br>2 O <sub>quinHA</sub> , 1<br>O <sub>OH</sub> ]] |  | Square<br>Pyramid | 1.28931 | 2.038 | 0.103 |

<sup>a</sup> Smallest CShM out of all ideal geometries from SHAPE v2.1 analysis.<sup>34</sup>

There are other examples of MCs formed with Zn<sup>2+</sup>, including [12-MC-4]s, [15-MC-5]s, and a bis[12-MC-4][12-MC-8] “encapsulated sandwich” compounds.<sup>24,38–45</sup> The structure reported here stands out among these examples since examples of [14-MC-5]s are rare and **Ln-1** series is only the second example reported. The first example of a [14-MC-5] was comprised of Mn<sup>3+</sup> and salicylhydroximate ligands that encapsulate a single Ln<sup>3+</sup> in their cavity, plus another Ln<sup>3+</sup> as a part of the MC ring.<sup>48</sup> Even though both compounds are [14-MC-5]s, there are significant differences in their structural compositions (**Figure 2**). Both [14-MC-5] compounds have a M–O–M “stutter” using a μ<sub>3</sub>-OH<sup>-</sup> or μ<sub>3</sub>-O<sup>2-</sup> rather than a hydroximate group that induces the removal of a nitrogen atom from the standard M–N–O–M motif. Another difference that can be observed



between the two structures is the presence of a mirror plane that bisects the molecule in  $\text{Mn}^{3+}/\text{Ln}^{3+}$  [14-MC-5] MC. Conversely, **Yb-1** does not possess a mirror plane and maintains the M–N–O sequence for each of the four subunits. In addition, the  $\text{Mn}^{3+}/\text{Ln}^{3+}$  MC has a  $\text{Ln}^{3+}$  in the [14-MC-5] MC ring, while that in the **Ln-1** consists only of  $\text{Zn}^{2+}$  ring metal ions. Lastly, the [14-MC-5] ring in  $\text{Mn}^{3+}$  is planar since each  $\text{Mn}^{3+}$  is located in an octahedral coordination environment with the 5,6-fused chelate motif of the salicylhydroximate ligand. In the case of **Ln-1**, both the square pyramidal  $\text{Zn}^{2+}$  centers and the 5,5-fused chelate motif requires some bowling to complete the cycle with reasonable bond lengths.



**Figure 2.** Molecular representation of [14-MC-5] motifs established from crystallographic data for the  $\text{Mn}^{3+}/\text{Y}^{3+}$  (a) and **Yb-1** (b) MCs. The MC ring and encapsulated  $\text{Ln}^{3+}$  are highlighted. Teal = Y, aqua = Yb, indigo = Mn, pink = Zn, light blue = N, red = O, grey = C.

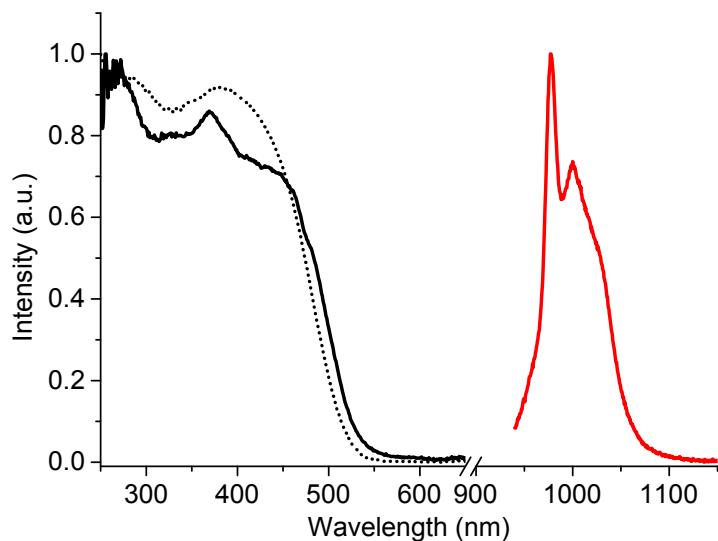
Absorption spectra were collected for each **Ln-1** and the parent ligands in *N,N*-dimethylformamide solution at ambient temperature (**Figure S4**, Supporting Information). Compared to the  $\text{H}_2\text{quinHA}$  and  $\text{H}_2\text{ph}$  that possess absorption bands in the UV range up to 350

and 300 nm, respectively, absorption spectra of **Ln-1** are significantly red-shifted and extend up to 475 nm. The broad lower energy absorption band with a maximum at 380 nm ( $\epsilon_{380} = 2.7 \times 10^4 \text{ M}^{-1} \text{ cm}^{-1}$ ) could be assigned to intra- and/or inter-ligand charge transfer (ILCT) transitions considering that  $\text{Zn}^{2+}$  usually does not participate in metal-to-ligand or ligand-to-metal charge transfer transitions and that the absorption spectra of **Ln-1** are independent of  $\text{Ln}^{3+}$  identity. Similar ILCT absorption bands were observed for  $\text{Zn}^{2+}/\text{Ln}^{3+}$  MCs with an ‘encapsulated sandwich’ structure assembled using quin $\text{HA}^{2-}$  ligands.<sup>24</sup> Diffuse reflectance spectra of **Ln-1** formed with the different  $\text{Ln}^{3+}$  are similar to each other and exhibit broad bands in the UV and visible range up to 550 nm (**Figure S5**, Supporting Information).

Luminescent properties of **Ln-1** were analyzed in the solid state. Energy positions of the ligand-centered levels, in particular triplet states, employ  $\text{Gd}^{3+}$  since the emissive state ( $32\,200 \text{ cm}^{-1}$ )<sup>49</sup> is too high in energy for many organic sensitizers. However, no phosphorescence could be detected upon excitation of **Gd-1** in the range of 280–340 nm at 77 K in time resolved mode. On the other hand, **Gd-1** exhibited broad-band emission in the range 450–750 nm arising from the ILCT in steady-state mode (**Figure S6**, Supporting Information). The energy position of the ILCT state was determined to be  $21\,410 \text{ cm}^{-1}$  (467 nm) from the onset of the emission band of **Gd-1**, a value

similar to the  $\text{Zn}^{2+}/\text{Ln}^{3+}$  ‘encapsulated sandwich’ MCs ( $21\,560\text{ cm}^{-1}$ ).<sup>24</sup> Upon excitation into ILCT band at 400 nm, **Tb-1** exhibited only a broad-band emission in the range 450–750 nm (**Figure S6**, Supporting Information). The latter could be explained by a high probability of back energy transfer because of the energy match between the ILCT ( $21\,410\text{ cm}^{-1}$ ) and the  $\text{Tb}^{3+}\ ^5\text{D}_4$  emitting level ( $20\,500\text{ cm}^{-1}$ ) in **Tb-1**. On the other hand, **Yb-1** upon excitation at 400 nm displays  $\text{Yb}^{3+}$ -centered luminescence in the near-infrared range due to the  $^2\text{F}_{5/2} \rightarrow ^2\text{F}_{7/2}$  transition (**Figure 3**). Excitation spectrum of **Yb-1** upon monitoring emission at 980 nm resembles the diffuse reflectance one (**Figure 3**, solid vs. dashed black traces) and exhibits broad bands in the UV and visible ranges up to 550 nm pointing towards a sensitization of  $\text{Yb}^{3+}$  through the MC scaffold.<sup>17</sup> It should be noted that  $\text{Yb}^{3+}$  near-infrared emission in **Yb-1** could be observed despite the presence of water molecules in the first coordination sphere of  $\text{Yb}^{3+}$  that often quench near-IR emitting  $\text{Ln}^{3+}$ .<sup>3</sup> The  $\text{Yb}^{3+}$ -centered absolute quantum yield ( $Q_{\text{Yb}}^{\text{L}}$ ) of **Yb-1** upon excitation at 400 nm is 0.051(1)%. Luminescence decays of **Yb-1** were best fitted by a monoexponential function (**Figure S7**) where the luminescence lifetime is 714(8) nanoseconds. Both values of  $Q_{\text{Yb}}^{\text{L}}$  and  $\tau_{\text{obs}}$  of **Yb-1** are smaller than the ones reported for the  $\text{Zn}^{2+}/\text{Yb}^{3+}$  ‘encapsulated sandwich’ MC ( $Q_{\text{Yb}}^{\text{L}} = 2.44(4)\%$ ;  $\tau = 47.8(4)$

ms),<sup>24</sup> due to the presence of water molecules directly bound to the lanthanide cation as well as self-quenching induced by proximal Yb<sup>3+</sup>.



**Figure 3.** Normalized steady-state luminescence spectra of **Yb-1**. Excitation spectra (black traces) were recorded with  $\lambda_{em} = 980$  nm. Emission spectra (red traces) were acquired with  $\lambda_{ex} = 400$  nm. The diffuse reflectance spectrum of **Yb-1** is superimposed for comparison (dashed black trace).

The new **Ln-1** MCs we report here represent a significant addition to the library of metallacrown structures not only as an example of a 14-MC-5 system, but also for the ability to sensitize near-IR emission from Yb<sup>3+</sup>. The compound is a fused bis[14-MC-5] that contains both quinHA<sup>2-</sup> and ph<sup>2-</sup>. Absorption spectra of **Ln-1** display broad bands at lower energy due to intra-/inter-ligand

charge transfer transitions. **Yb-1** in the solid-state displays characteristic  $\text{Yb}^{3+}$  emission in the near-IR range despite the presence of water molecules directly bound to the metal ion. Given the novelty of the structure and composition as well as the potential application of near-IR luminescence, **Ln-1** is a notable MC compound.

## ASSOCIATED CONTENT

The following files are available free of charge.

Electronic Supplementary Information (ESI) available containing experimental details, additional spectroscopic information, and crystallographic parameters in word document format.

Single crystal diffraction data are available for **Yb-1** in CIF format free of charge from [www.ccdc.cam.ac.uk](http://www.ccdc.cam.ac.uk) using deposition number 2125941.

## AUTHOR INFORMATION

### Corresponding Authors

\* Svetlana V. Eliseeva (email: [svetlana.eliseeva@cnrs.fr](mailto:svetlana.eliseeva@cnrs.fr)), Stéphane Petoud (email: [stephane.petoud@inserm.fr](mailto:stephane.petoud@inserm.fr)) and Jacob C. Lutter (email: [jclutter@umich.edu](mailto:jclutter@umich.edu))

## **Author Contributions**

The manuscript was written through contributions of all authors. All authors have given approval to the final version of the manuscript.

## **Funding Sources**

Funding was provided by Wayne State University, the National Institutes of Health, La Ligue Contre le Cancer, Molécules Marines Métabolisme et Cancer from the Cancéropôle Grand Ouest, and the Institut National de la Santé et de la Recherche Médicale (INSERM).

## **Notes**

The authors have no conflicts of interest to declare.

## **ACKNOWLEDGMENT**

JCL acknowledges support from Wayne State University, MJA acknowledges support from the National Institutes of Health (EB027103). The work in France was supported by La Ligue Contre le Cancer (Comité du Loiret et d'Eure-et-Loir) and the network Molécules Marines, Métabolisme et Cancer from the Cancéropôle Grand Ouest. S.P. acknowledges support from the Institut National de la Santé et de la Recherche Médicale (INSERM).

## SUPPORTING INFORMATION

The Supporting Information available:

Experimental details, additional spectroscopic information and crystallographic parameters (in PDF format).

Single crystal diffraction data are available for **Yb-1** in CIF format free of charge from [www.ccdc.cam.ac.uk](http://www.ccdc.cam.ac.uk) using deposition number 2125941.

## ABBREVIATIONS

MC, metallocrown; Ln<sup>3+</sup>, lanthanide; H<sub>2</sub>quinHA, quinaldic hydroxamic acid; H<sub>2</sub>ph, phthalic acid.

## REFERENCES

- (1) Sorace, L.; Gatteschi, D. Electronic Structure and Magnetic Properties of Lanthanide Molecular Complexes. In *Lanthanides and Actinides in Molecular Magnetism*; Wiley-VCH Verlag GmbH & Co. KGaA: Weinheim, Germany, 2015; pp 1–26.  
<https://doi.org/10.1002/9783527673476.ch1>.
- (2) Bünzli, J.-C. G.; Eliseeva, S. V. Photophysics of Lanthanoid Coordination Compounds. In *Comprehensive Inorganic Chemistry II*; Yam, V. W.-W., Ed.; Elsevier: Amsterdam, 2013;



pp 339–398. <https://doi.org/10.1016/B978-0-08-097774-4.00803-2>.

- (3) Bünzli, J.-C. G.; Eliseeva, S. V. Basics of Lanthanide Photophysics. In *Lanthanide Luminescence: Photophysical, Analytical and Biological Aspects*; Hanninen, P., Harma, H., Eds.; Springer: Berlin, 2010; pp 1–45. [https://doi.org/10.1007/4243\\_2010\\_3](https://doi.org/10.1007/4243_2010_3).
- (4) Rinehart, J. D.; Long, J. R. Exploiting Single-Ion Anisotropy in the Design of f-Element Single-Molecule Magnets. *Chem. Sci.* **2011**, *2* (11), 2078. <https://doi.org/10.1039/c1sc00513h>.
- (5) *Contrast Agents for MRI*; Pierre, V. C., Allen, M. J., Eds.; New Developments in NMR; Royal Society of Chemistry: Cambridge, 2017. <https://doi.org/10.1039/9781788010146>.
- (6) Harnden, A. C.; Parker, D.; Rogers, N. J. Employing Paramagnetic Shift for Responsive MRI Probes. *Coord. Chem. Rev.* **2019**, *383*, 30–42. <https://doi.org/10.1016/j.ccr.2018.12.012>.
- (7) Parker, D.; Suturina, E. A.; Kuprov, I.; Chilton, N. F. How the Ligand Field in Lanthanide Coordination Complexes Determines Magnetic Susceptibility Anisotropy, Paramagnetic NMR Shift, and Relaxation Behavior. *Acc. Chem. Res.* **2020**, *53* (8), 1520–1534.

<https://doi.org/10.1021/acs.accounts.0c00275>.

- (8) Werner, E. J.; Datta, A.; Jocher, C. J.; Raymond, K. N. High-Relaxivity MRI Contrast Agents: Where Coordination Chemistry Meets Medical Imaging. *Angew. Chemie Int. Ed.* **2008**, *47*(45), 8568–8580. <https://doi.org/10.1002/anie.200800212>.
- (9) Li, H.; Meade, T. J. Molecular Magnetic Resonance Imaging with Gd(III)-Based Contrast Agents: Challenges and Key Advances. *J. Am. Chem. Soc.* **2019**, *141* (43), 17025–17041. <https://doi.org/10.1021/jacs.9b09149>.
- (10) Bünzli, J. C. G.; Eliseeva, S. V. Lanthanide NIR Luminescence for Telecommunications, Bioanalyses and Solar Energy Conversion. *J. Rare Earths* **2010**, *28* (6), 824–842. [https://doi.org/10.1016/S1002-0721\(09\)60208-8](https://doi.org/10.1016/S1002-0721(09)60208-8).
- (11) Gao, R.; Kodaimati, M. S.; Yan, D. Recent Advances in Persistent Luminescence Based on Molecular Hybrid Materials. *Chem. Soc. Rev.* **2021**, *50* (9), 5564–5589. <https://doi.org/10.1039/D0CS01463J>.
- (12) Gao, R.; Zhao, M.; Guan, Y.; Fang, X.; Li, X.; Yan, D. Ordered and Flexible Lanthanide Complex Thin Films Showing Up-Conversion and Color-Tunable Luminescence. *J. Mater.*

- Chem. C* **2014**, *2*(45), 9579–9586. <https://doi.org/10.1039/C4TC01213E>.
- (13) Yang, Y.; Wang, K.-Z.; Yan, D. Smart Luminescent Coordination Polymers toward Multimode Logic Gates: Time-Resolved, Tribochromic and Excitation-Dependent Fluorescence/Phosphorescence Emission. *ACS Appl. Mater. Interfaces* **2017**, *9* (20), 17399–17407. <https://doi.org/10.1021/acsami.7b00594>.
- (14) Yang, Y.; Wang, K.-Z.; Yan, D. Lanthanide Doped Coordination Polymers with Tunable Afterglow Based on Phosphorescence Energy Transfer. *Chem. Commun.* **2017**, *53* (55), 7752–7755. <https://doi.org/10.1039/C7CC04356B>.
- (15) Yang, X.; Lin, X.; Zhao, Y.; Zhao, Y. S.; Yan, D. Lanthanide Metal-Organic Framework Microrods: Colored Optical Waveguides and Chiral Polarized Emission. *Angew. Chemie Int. Ed.* **2017**, *56*(27), 7853–7857. <https://doi.org/10.1002/anie.201703917>.
- (16) Weissman, S. I. Intramolecular Energy Transfer The Fluorescence of Complexes of Europium. *J. Chem. Phys.* **1942**, *10*(4), 214–217. <https://doi.org/10.1063/1.1723709>.
- (17) Uh, H.; Petoud, S. Novel Antennae for the Sensitization of near Infrared Luminescent Lanthanide Cations. *Comptes Rendus Chim.* **2010**, *13* (6–7), 668–680.

<https://doi.org/10.1016/j.crci.2010.05.007>.

- (18) Lah, M. S.; Kirk, M. L.; Hatfield, W.; Pecoraro, V. L. The Tetranuclear Cluster  $\text{Fe}^{\text{III}}[\text{Fe}^{\text{III}}(\text{Salicylhydroximato})(\text{MeOH})(\text{Acetate})]_3$  Is an Analogue of  $\text{M}^{3+}(\text{9-Crown-3})$ . *J. Chem. Soc. Chem. Commun.* **1989**, No. 21, 1606. <https://doi.org/10.1039/c39890001606>.
- (19) Pecoraro, V. L. Structural Characterization of  $[\text{VO}(\text{Salicylhydroximate})(\text{CH}_3\text{OH})]_3$ : Applications to the Biological Chemistry of Vanadium(V). *Inorganica Chim. Acta* **1989**, *155* (2), 171–173. [https://doi.org/10.1016/S0020-1693\(00\)90405-5](https://doi.org/10.1016/S0020-1693(00)90405-5).
- (20) Mezei, G.; Zaleski, C. M.; Pecoraro, V. L. Structural and Functional Evolutions of Metallacrowns. *Chem. Rev.* **2007**, *107* (11), 4933–5003. <https://doi.org/10.1021/cr078200h>.
- (21) Chow, C. Y.; Trivedi, E. R.; Pecoraro, V.; Zaleski, C. M. Heterometallic Mixed *3d-4f* Metallacrowns: Structural Versatility, Luminescence, and Molecular Magnetism. *Comments Inorg. Chem.* **2015**, *35* (4), 214–253. <https://doi.org/10.1080/02603594.2014.981811>.
- (22) Lutter, J. C.; Zaleski, C. M.; Pecoraro, V. L. Metallacrowns: Supramolecular Constructs

- With Potential in Extended Solids, Solution-State Dynamics, Molecular Magnetism, and Imaging. In *Advances in Inorganic Chemistry*, Eldik, R. van, Puchta, R., Eds.; Academic Press, 2018; Vol. 71, pp 177–246. <https://doi.org/10.1016/bs.adioch.2017.11.007>.
- (23) Jankolovits, J.; Andolina, C. M.; Kampf, J. W.; Raymond, K. N.; Pecoraro, V. L. Assembly of Near-Infrared Luminescent Lanthanide Host(Host-Guest) Complexes With a Metallocrown Sandwich Motif. *Angew. Chemie Int. Ed.* **2011**, *50* (41), 9660–9664. <https://doi.org/10.1002/anie.201103851>.
- (24) Trivedi, E. R.; Eliseeva, S. V.; Jankolovits, J.; Olmstead, M. M.; Petoud, S.; Pecoraro, V. L. Highly Emitting Near-Infrared Lanthanide “Encapsulated Sandwich” Metallocrown Complexes with Excitation Shifted toward Lower Energy. *J. Am. Chem. Soc.* **2014**, *136* (4), 1526–1534. <https://doi.org/10.1021/ja4113337>.
- (25) Chow, C. Y.; Eliseeva, S. V.; Trivedi, E. R.; Nguyen, T. N.; Kampf, J. W.; Petoud, S.; Pecoraro, V. L. Ga<sup>3+</sup>/Ln<sup>3+</sup> Metallocrowns: A Promising Family of Highly Luminescent Lanthanide Complexes That Covers Visible and Near-Infrared Domains. *J. Am. Chem. Soc.* **2016**, *138* (15), 5100–5109. <https://doi.org/10.1021/jacs.6b00984>.

- (26) Nguyen, T. N.; Chow, C. Y.; Eliseeva, S. V.; Trivedi, E. R.; Kampf, J. W.; Martinić, I.; Petoud, S.; Pecoraro, V. L. One-Step Assembly of Visible and Near-Infrared Emitting Metallacrown Dimers Using a Bifunctional Linker. *Chem. Eur. J.* **2018**, *24*(5), 1031–1035. <https://doi.org/10.1002/chem.201703911>.
- (27) Martinić, I.; Eliseeva, S. V.; Nguyen, T. N.; Pecoraro, V. L.; Petoud, S. Near-Infrared Optical Imaging of Necrotic Cells by Photostable Lanthanide-Based Metallacrowns. *J. Am. Chem. Soc.* **2017**, *139*(25), 8388–8391. <https://doi.org/10.1021/jacs.7b01587>.
- (28) Martinić, I.; Eliseeva, S. V.; Nguyen, T. N.; Foucher, F.; Gosset, D.; Westall, F.; Pecoraro, V. L.; Petoud, S. Near-Infrared Luminescent Metallacrowns for Combined in Vitro Cell Fixation and Counter Staining. *Chem. Sci.* **2017**, *8* (9), 6042–6050. <https://doi.org/10.1039/C7SC01872J>.
- (29) Lutter, J. C.; Eliseeva, S. V.; Kampf, J. W.; Petoud, S.; Pecoraro, V. L. A Unique Ln<sup>III</sup>{[3.3.1]Ga<sup>III</sup> Metallacryptate} Series That Possesses Properties of Slow Magnetic Relaxation and Visible/Near-Infrared Luminescence. *Chem. Eur. J.* **2018**, *24*(42), 10773–10783. <https://doi.org/10.1002/chem.201801355>.

- (30) Lutter, J. C.; Eliseeva, S. V.; Collet, G.; Martinić, I.; Kampf, J. W.; Schneider, B. L.; Carichner, A.; Sobilo, J.; Lerondel, S.; Petoud, S.; Pecoraro, V. L. Iodinated Metallacrowns: Toward Combined Bimodal Near-Infrared and X-Ray Contrast Imaging Agents. *Chem. Eur. J.* **2020**, *26* (6), 1274–1277. <https://doi.org/10.1002/chem.201905241>.
- (31) Lutter, J. C.; Lopez Bermudez, B. A.; Nguyen, T. N.; Kampf, J. W.; Pecoraro, V. L. Functionalization of Luminescent Lanthanide-Gallium Metallacrowns Using Copper-Catalyzed Alkyne-Azide Cycloaddition and Thiol-Maleimide Michael Addition. *J. Inorg. Biochem.* **2019**, *192* (October 2018), 119–125. <https://doi.org/10.1016/j.jinorgbio.2018.12.011>.
- (32) Salerno, E. V.; Zeler, J.; Eliseeva, S. V.; Hernández-Rodríguez, M. A.; Carneiro Neto, A. N.; Petoud, S.; Pecoraro, V. L.; Carlos, L. D.  $[\text{Ga}^{3+}_8\text{Sm}^{3+}_2, \text{Ga}^{3+}_8\text{Tb}^{3+}_2]$  Metallacrowns Are Highly Promising Ratiometric Luminescent Molecular Nanothermometers Operating at Physiologically Relevant Temperatures. *Chem. Eur. J.* **2020**, *26* (61), 13792–13796. <https://doi.org/10.1002/chem.202003239>.
- (33) Eliseeva, S. V.; Salerno, E. V.; Lopez Bermudez, B. A.; Petoud, S.; Pecoraro, V. L.  $\text{Dy}^{3+}$

- White Light Emission Can Be Finely Controlled by Tuning the First Coordination Sphere of Ga<sup>3+</sup>/Dy<sup>3+</sup> Metallacrown Complexes. *J. Am. Chem. Soc.* **2020**, *142* (38), 16173–16176.  
<https://doi.org/10.1021/jacs.0c07198>.
- (34) Llunell, M.; Casanova, D.; Cicera, J.; Alemany, P.; Alvarez, S. SHAPE version 2.1. Barcelona, Spain 2013.
- (35) Trzesowska, A.; Kruszynski, R.; Bartczak, T. J. New Bond-Valence Parameters for Lanthanides. *Acta Crystallogr. Sect. B Struct. Sci.* **2004**, *60* (2), 174–178.  
<https://doi.org/10.1107/S0108768104002678>.
- (36) Zheng, H.; Langner, K. M.; Shields, G. P.; Hou, J.; Kowiel, M.; Allen, F. H.; Murshudov, G.; Minor, W. Data Mining of Iron(II) and Iron(III) Bond-Valence Parameters, and Their Relevance for Macromolecular Crystallography. *Acta Crystallogr. Sect. D Struct. Biol.* **2017**, *73* (4), 316–325. <https://doi.org/10.1107/S2059798317000584>.
- (37) Addison, A. W.; Rao, T. N.; Reedijk, J.; van Rijn, J.; Verschoor, G. C. Synthesis, Structure, and Spectroscopic Properties of Copper(II) Compounds Containing Nitrogen–Sulphur Donor Ligands; the Crystal and Molecular Structure of Aqua[1,7-Bis(N-



- Methylbenzimidazol-2'-yl)-2,6-Dithiaheptane]Copper(II) Perchlorate. *J. Chem. Soc., Dalton Trans.* **1984**, No. 7, 1349–1356. <https://doi.org/10.1039/DT9840001349>.
- (38) Alexiou, M.; Dendrinou-Samara, C.; Raptopoulou, C. P.; Terzis, A.; Kessissoglou, D. P. From Monomer Zinc–Oxamate Complexes to Tetranuclear Inverse 12-Membered and Octanuclear 12-Membered Metallacrowns. *Inorg. Chem.* **2002**, *41* (18), 4732–4738. <https://doi.org/10.1021/ic0200904>.
- (39) Alexiou, M.; Katsoulakou, E.; Dendrinou-Samara, C.; Raptopoulou, C. P.; Psycharis, V.; Manessi-Zoupa, E.; Perlepes, S. P.; Kessissoglou, D. P. Di-2-pyridyl Ketone Oxime in Zinc Chemistry: Inverse 12-Metallacrown-4 Complexes and Cationic Pentanuclear Clusters. *Eur. J. Inorg. Chem.* **2005**, *2005* (10), 1964–1978. <https://doi.org/10.1002/ejic.200400933>.
- (40) Ostrowska, M.; Golenya, I. A.; Haukka, M.; Fritsky, I. O.; Gumienna-Kontecka, E. Complex Formation of Copper(II), Nickel(II) and Zinc(II) with Ethylophosphonoacetohydroxamic Acid: Solution Speciation, Synthesis and Structural Characterization. *New J. Chem.* **2019**, *43* (26), 10237–10249. <https://doi.org/10.1039/C9NJ01175G>.

- (41) Marchiò, L.; Marchetti, N.; Atzeri, C.; Borghesani, V.; Remelli, M.; Tegoni, M. The Peculiar Behavior of Picha in the Formation of Metallacrown Complexes with Cu(II), Ni(II) and Zn(II) in Aqueous Solution. *Dalton Trans.* **2015**, *44* (7), 3237–3250. <https://doi.org/10.1039/C4DT03264K>.
- (42) Jankolovits, J.; Kampf, J. W.; Pecoraro, V. L. Insight into the Structural Versatility of the Ln(III)[15-Metallacrown-5] Platform by Comparing Analogs with Ni(II), Cu(II), and Zn(II) Ring Ions. *Polyhedron* **2013**, *52*, 491–499. <https://doi.org/10.1016/j.poly.2012.08.046>.
- (43) Jankolovits, J.; Kampf, J. W.; Pecoraro, V. L. Solvent Dependent Assembly of Lanthanide Metallacrowns Using Building Blocks with Incompatible Symmetry Preferences. *Inorg. Chem.* **2014**, *53* (14), 7534–7546. <https://doi.org/10.1021/ic500832u>.
- (44) Jankolovits, J.; Kampf, J. W.; Pecoraro, V. L. Assembly of Zinc Metallacrowns with an  $\alpha$ -Amino Hydroxamic Acid Ligand. *Chinese Chem. Lett.* **2015**, *26* (4), 444–448. <https://doi.org/10.1016/j.ccllet.2015.01.017>.
- (45) Li, Q.-W.; Liu, J.-L.; Jia, J.-H.; Chen, Y.-C.; Liu, J.; Wang, L.-F.; Tong, M.-L. “Half-Sandwich” Yb<sup>III</sup> Single-Ion Magnets with Metallacrowns. *Chem. Commun.* **2015**, *51* (51),

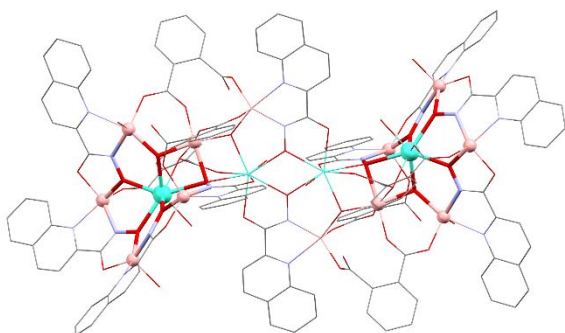
10291–10294. <https://doi.org/10.1039/C5CC03389F>.

- (46) Boron, T. T.; Lutter, J. C.; Daly, C. I.; Chow, C. Y.; Davis, A. H.; Nimthong-Roldán, A.; Zeller, M.; Kampf, J. W.; Zaleski, C. M.; Pecoraro, V. L. The Nature of the Bridging Anion Controls the Single-Molecule Magnetic Properties of DyX<sub>4</sub>M<sub>12</sub>-Metallacrown-4 Complexes. *Inorg. Chem.* **2016**, *55* (20), 10597–10607. <https://doi.org/10.1021/acs.inorgchem.6b01832>.
- (47) Chow, C. Y.; Guillot, R.; Rivière, E.; Kampf, J. W.; Mallah, T.; Pecoraro, V. L. Synthesis and Magnetic Characterization of Fe(III)-Based 9-Metallacrown-3 Complexes Which Exhibit Magnetorefrigerant Properties. *Inorg. Chem.* **2016**, *55* (20), 10238–10247. <https://doi.org/10.1021/acs.inorgchem.6b01404>.
- (48) Boron, T. T.; Kampf, J. W.; Pecoraro, V. L. A Mixed 3d-4f 14-Metallacrown-5 Complex That Displays Slow Magnetic Relaxation through Geometric Control of Magnetoanisotropy. *Inorg. Chem.* **2010**, *49* (20), 9104–9106. <https://doi.org/10.1021/ic101121d>.
- (49) Carnall, W. T.; Fields, P. R.; Rajnak, K. Electronic Energy Levels of the Trivalent

Lanthanide Aquo Ions. II.  $Gd^{3+}$ . *J. Chem. Phys.* **1968**, *49* (10), 4443–4446.

<https://doi.org/10.1063/1.1669894>.

## Table of Contents Synopsis



A fused set of rarely observed 14-metallacrown-5 moieties is described using single-crystal X-ray diffraction data, and near-infrared emission from  $\text{Yb}^{3+}$  is observed in the solid state.